

Simulation study for adsorption-induced structural transition in stacked-layer porous coordination polymers: Equilibrium and hysteretic adsorption behaviors

Ryohei Numaguchi, Hideki Tanaka, Satoshi Watanabe, and Minoru T. Miyahara

Citation: *The Journal of Chemical Physics* **138**, 054708 (2013); doi: 10.1063/1.4789810

View online: <http://dx.doi.org/10.1063/1.4789810>

View Table of Contents: <http://scitation.aip.org/content/aip/journal/jcp/138/5?ver=pdfcov>

Published by the [AIP Publishing](#)

Articles you may be interested in

[Dependence of adsorption-induced structural transition on framework structure of porous coordination polymers](#)
J. Chem. Phys. **140**, 044707 (2014); 10.1063/1.4862735

[Understanding adsorption-induced structural transitions in metal-organic frameworks: From the unit cell to the crystal](#)
J. Chem. Phys. **137**, 184702 (2012); 10.1063/1.4765369

[Free energy landscapes for the thermodynamic understanding of adsorption-induced deformations and structural transitions in porous materials](#)
J. Chem. Phys. **137**, 044118 (2012); 10.1063/1.4738776

[Osmotic ensemble methods for predicting adsorption-induced structural transitions in nanoporous materials using molecular simulations](#)
J. Chem. Phys. **134**, 184103 (2011); 10.1063/1.3586807

[Free energy analysis for adsorption-induced lattice transition of flexible coordination framework](#)
J. Chem. Phys. **130**, 164707 (2009); 10.1063/1.3122988



Re-register for Table of Content Alerts

Create a profile.



Sign up today!



Simulation study for adsorption-induced structural transition in stacked-layer porous coordination polymers: Equilibrium and hysteretic adsorption behaviors

Ryohei Numaguchi, Hideki Tanaka, Satoshi Watanabe, and Minoru T. Miyahara^{a)}
 Department of Chemical Engineering, Kyoto University, Katsura, Nishikyo, Kyoto 615-8510, Japan

(Received 2 November 2012; accepted 15 January 2013; published online 7 February 2013)

We conduct grand canonical Monte Carlo simulations and a free-energy analysis for a simplified model of a stacked-layer porous coordination polymer to understand the gate phenomenon, which is a structural transition of a host framework induced by the adsorption of guest particles. Our calculations demonstrate that stabilization of the system due to the guest adsorption causes host deformation under thermodynamic equilibrium. We also investigate spontaneous transition behaviors (gate opening and closing under metastable conditions). The structural transition should occur when the required activation energy, which is determined using the free-energy analysis, becomes equal to the system energy fluctuation. To estimate the system energy fluctuation, we construct a kinetic transition model based on the transition state theory. In this model, the system energy fluctuation can be calculated by setting the adsorption time and transition domain size of the host framework. The model demonstrates that a smaller domain size results in a gate-opening transition at lower pressure. Furthermore, we reveal that the slope of the logarithm of the equilibrium structural transition pressure versus reciprocal temperature shows transition enthalpy, and that slopes of the gate-opening and -closing transition pressures versus reciprocal temperature show activation enthalpies. © 2013 American Institute of Physics. [<http://dx.doi.org/10.1063/1.4789810>]

I. INTRODUCTION

Porous coordination polymer (PCP), also known as metal-organic framework (MOF), is a new class of nanoporous materials constructed of metal ions and organic linkers.^{1–3} Particularly, some types of PCPs, called soft porous crystals,⁴ have a dynamic structure that results in a peculiar adsorption behavior known as breathing or the gate phenomenon, in which, at a certain pressure, guest molecules are adsorbed abruptly, causing structural deformation of the host (gate opening), and are desorbed when the pressure drops below the gate-opening pressure (gate closing), restoring the shape of the host. This phenomenon has been reported for several motifs of soft PCPs such as one-dimensional channels,^{5–8} two-dimensional stacked-layers,^{9–19} and interpenetrating three-dimensional motifs.^{20–22} Intriguingly, this gating behavior is tunable with the functionalization of the organic linkers^{8,14} and replacement of the metal ions.¹⁶ This stimulus-responsive transition behavior suggests potential application to various adsorption technologies such as gas storage,^{17,23} separation,^{18,24} sensors,²⁵ nano flasks for topotactic radical polymerization,²⁶ and carriers for drug delivery.²⁷ To understand the gate phenomenon, an *in situ* X-ray diffraction experiment for CO₂ adsorption onto MIL-53 was conducted,²⁸ and it showed that only two lattice structures, namely, the narrow-pore (*np*) and large-pore (*lp*) phases, appeared during the structural transition, which indicates that the phenomenon can be at-

tributed to first-order adsorption-induced structural transition. The adsorption-induced structural transition was also experimentally observed for the other host/guest systems such as montmorillonite clay/water,^{29–33} zeolites/aromatics,^{34,35} alkali earth halides/ammonia,^{36–38} and anthracenebisresorcinol crystal/ethyl acetate.³⁹ However, the microscopic mechanism of the adsorption-induced structural transition remains to be fully understood.

Computational approaches have provided useful information to understand the deformation of porous materials due to guest adsorption. In the 1980s, Megan and Snook^{40,41} and Lane and Spurling⁴² predicted that the solvation pressure of a confined Lennard-Jones (LJ) fluid in a slit pore composed of LJ atoms oscillates with an increase in the slit width. Accordingly, Israelachvili *et al.*^{43,44} performed a surface force measurement of confined octamethylcyclotetrasiloxane [(CH₃)₂SiO]₄ between mica substrates and confirmed the oscillation of the solvation pressure. Since then, many computational studies of structural deformation in a slit system have been reported. Most molecular simulations have been conducted in the canonical or the grand canonical ensembles in the first decade,^{45–56} and new ensembles such as isostress-isostrain,⁵¹ grand isostress,^{50,51} grand isoshear,⁵⁴ and grand isoforce ensembles⁵⁴ have been developed to examine the stress-strain correlation in slit systems. To investigate swelling in the clay/water system, molecular simulations have been conducted in the isostress ensemble^{57–65} and the grand canonical ensemble.^{58,64–67} Those simulations in the isostress ensemble succeeded in predicting a stable clay/water structure; however, the stepwise adsorption isotherm based on the structural transition of the host was not reported, because

^{a)} Author to whom correspondence should be addressed. Electronic mail: miyahara@cheme.kyoto-u.ac.jp.

additional calculation is required to obtain a bulk gas pressure in equilibrium with the adsorbed phase. This stepwise adsorption isotherm was also not represented by the molecular simulation in the grand canonical ensemble, because it does not allow one to determine the thermodynamically stable structures in clay/water systems with different interlayer spacing. To describe the adsorption-induced structural transition, the most appropriate ensemble is an osmotic ensemble ($N_{\text{host}}, \mu, \sigma, T$), where the control parameters are the number of atoms in the host framework N_{host} , the chemical potential of the adsorbed fluid μ , the mechanical constraint σ (which is simply the external pressure in an isotropic system), and the temperature T . A molecular simulation study with this ensemble for the adsorption-induced structural transition was first conducted by Ghoufi *et al.*^{68,69} Their hybrid osmotic Monte Carlo simulation for the MIL-53/CO₂ system successfully explained the structural transition from the *np* phase to the *lp* phase, but it failed to explain the *lp* → *np* transition because of difficulty in sampling the full phase space.

Coudert *et al.*^{70,71} proposed an analytical approach using a general thermodynamic scheme for predicting the equilibrium behavior of the structural transition of PCPs. They calculated the pressure dependence of the osmotic free energies in the pre- and the post-transition states by thermodynamic integration of the Langmuir isotherms, which are obtained by fitting to the corresponding parts of the experimental adsorption isotherm. They determined the host deformation energy, ΔF^{host} , so that the intersection of the two free-energy profiles coincided with the experimental transition pressure. This model could explain the conditions for the occurrence of the structural transition, and they successfully derived a phase diagram for the MIL-53/xenon system;⁷² however, their model could not explain the hysteresis phenomenon. To predict the hysteretic behavior, Neimark *et al.*⁷³ proposed a stress-based model in which the structural transition occurs when the adsorption stress, which is applied on account of guest adsorption, approaches a certain critical stress. This model was applied in experimental^{74,75} and simulation⁷⁶ studies for the MIL-53/guest system, and it gave an insight into specific hysteretic behavior; however, it was not sufficient for quantitative prediction of the spontaneous transition pressures. A comprehensive review of analytical approaches and direct simulations for the osmotic ensemble is found in Ref. 77.

Free-energy analysis is another method to determine the structural transition behavior.^{78,79} This method is neither a direct simulation of the structural deformation, nor an analytical approach, but a combination of the two. Its methodology is as follows: First, the adsorption stress is calculated with the grand canonical Monte Carlo (GCMC) simulation. Second, the adsorption stress is integrated with respect to the change in system volume to obtain the relative osmotic free energy. Finally, the most stable state is determined based on the obtained osmotic free-energy landscape. This method has been applied to the LJ slit system,⁵⁰ clay materials,^{80–88} simple models of MIL-53,⁸⁹ and mutually interpenetrating PCP.^{78,79} The osmotic free energy can be also obtained by another pathway, i.e., the integration of the adsorption isotherm with respect to the chemical potential, and this method has been applied to investigate the adsorption-induced structural

transition of zeolites.^{90–92} In contrast to the direct simulation method, free-energy analysis can represent the equilibrium behavior of the adsorption-induced structural transition successfully, but there are some limitations. One is the impossibility of reproducing the dynamics of the deformation, and the other is the difficulty of quantitatively determining the hysteretic behavior. Watanabe *et al.*⁷⁸ determined the hysteretic transition pressure with the activation energy of the structural transition obtained from the free-energy landscape by assuming energy fluctuation in the system. However, the amount of the energy fluctuation cannot be determined by free-energy analysis, because the energy fluctuation depends on observation time.

In the present study, we conducted GCMC simulations and free-energy analysis for a simplified model of stacked-layer PCP. The simplification of the model allows us to elucidate the physical essence of the gate phenomenon. We obtained the relative osmotic free energy from the two thermodynamic integration pathways. The adsorption stress was calculated from three newly derived equations for the stacked-layer system. The equilibrium structural transition behavior was determined from the free-energy profiles, and furthermore, the hysteretic transition pressures were predicted by the relationship between the activation energy and the assumed system energy fluctuation. Temperature dependence of the equilibrium pressure and spontaneous gate-opening and -closing transition pressures was also investigated. To estimate the system energy fluctuation, we propose a kinetic transition model, in which a PCP crystal is composed of transition domains, which can deform independently of each other. Based on the model, we calculated a rate constant for the structural transition using transition state theory^{93–95} and associated the energy fluctuation with the adsorption time and the size of the transition domain. We also revealed that equilibrium transition enthalpy and gate-opening and -closing activation enthalpies can be obtained from the slopes of the logarithms of the transition pressures $\ln P$ versus reciprocal temperature T^{-1} , respectively. This gives a clear understanding about the experimental results that the $\ln P$ vs. T^{-1} plot has a linear correlation.^{6,8,11,12,96}

II. METHODS

A. Model and simulation details

To elucidate the physical essence of the gate phenomenon, we constructed a simplified model of a stacked-layer PCP for which the structural transition has been observed experimentally.^{9–19} Figure 1(a) shows a typical layer structure of a stacked-layer PCP (ELM-11¹³), which has a grid network formed by coordination bonds between metal ions and linker molecules. Pillaring anions are located on both sides of the layer. In our model, the layer was assumed as a rigid smeared-atom wall, and the pillars were located on the one side of the layers (Fig. 1(b)). The simulation box was composed of seven stacked unit cells containing one layer each (Fig. 1(c)). The center-to-center distance between the two layers was defined as the interlayer width h . The interlayer widths for all the neighboring layers were assumed

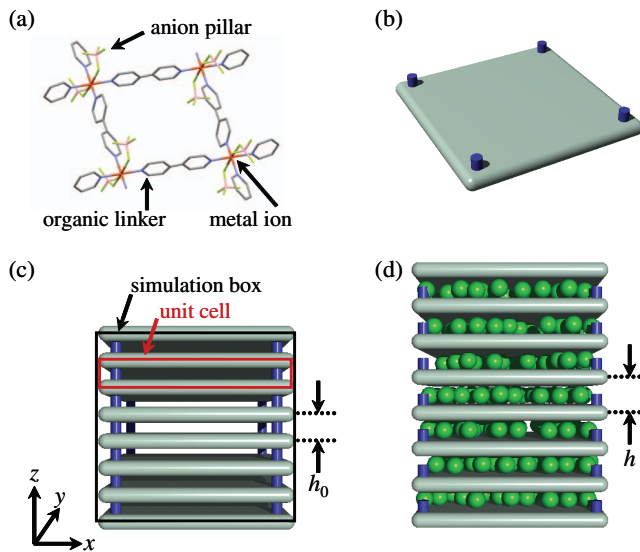


FIG. 1. (a) Two-dimensional sheet of the stacked-layer PCP, ELM-11 (see Ref. 13), consisting of metal ions, organic linkers, and anion pillars on the layer. (b) Simplified model of the stacked-layer PCP, which is composed of a smeared-atom layer and pillars on the layer. (c) Simulation box including the seven unit cells with interlayer width h_0 . (d) Snapshot of the guest molecules in the simulation box after the gate opening.

to remain the same when the interlayer width expanded as the guest molecules were adsorbed in the interlayer spaces (Fig. 1(d)). For a description of fluid-fluid interaction u^{ff} , the 12-6 LJ potential was used

$$u^{\text{ff}}(r_{ij}) = 4\epsilon_{\text{ff}} \left\{ \left(\frac{\sigma_{\text{ff}}}{r_{ij}} \right)^{12} - \left(\frac{\sigma_{\text{ff}}}{r_{ij}} \right)^6 \right\}, \quad (1)$$

where r_{ij} is the pairwise distance between the guest molecules. The guest molecule was LJ argon with $\sigma_{\text{ff}} = 0.341$ nm and $\epsilon_{\text{ff}}/k_{\text{B}} = 119.8$ K, where k_{B} is the Boltzmann constant. For fluid-solid interaction u^{fs} , the 10-4 LJ potential was used

$$u^{\text{fs}}(z_{ik}) = 2\pi\rho_{\text{s}}\epsilon_{\text{fs}}\sigma_{\text{fs}}^2 \left\{ \frac{2}{5} \left(\frac{\sigma_{\text{fs}}}{z_{ik}} \right)^{10} - \left(\frac{\sigma_{\text{fs}}}{z_{ik}} \right)^4 \right\}, \quad (2)$$

where z_{ik} denotes a distance between the i th fluid molecule and the k th layer. The layers were composed of carbon atoms with LJ parameters of $\sigma_{\text{ss}} = 0.340$ nm and $\epsilon_{\text{ss}}/k_{\text{B}} = 28$ K. The atomic number density of the layer, ρ_{s}^* ($=\rho_{\text{s}}\sigma_{\text{ff}}^2$), was set at 2.2 to attain approximately the same atomic density as ELM-11.¹³ The LJ parameters, σ_{fs} and ϵ_{fs} , were calculated following the Lorentz-Berthelot mixing rules. A layer-layer interaction u^{ll} is represented by Eq. (3), which is derived from an area integral of the 10-4 LJ potential

$$u^{\text{ll}}(h_{kl}) = 2\pi\rho_{\text{s}}^2\epsilon_{\text{ss}}\sigma_{\text{ss}}^2 \left\{ \frac{2}{5} \left(\frac{\sigma_{\text{ss}}}{h_{kl}} \right)^{10} - \left(\frac{\sigma_{\text{ss}}}{h_{kl}} \right)^4 \right\}, \quad (3)$$

where h_{kl} is the distance between the k th and the l th layers. The derivation of Eq. (3) is described in the supplementary material.⁹⁷ Pillar-pillar interaction u^{pp} and layer-pillar interaction u^{lp} were set to be the 12-6 LJ and the 10-4 LJ potentials, respectively. The LJ parameters of the pillar were the same with those of the guest molecule, and density of the pillar was

set to be $1/(100\sigma_{\text{ff}}^2)$. Interactions between the pillars and the guest molecules were neglected because of the low density of the pillars. All the potentials were cut and shifted

$$u(R) = \begin{cases} u(R) - u(r_{\text{c}}) & \text{at } R \leq r_{\text{c}} \\ 0 & \text{at } R > r_{\text{c}} \end{cases}, \quad (4)$$

where the cut-off distance r_{c} was set at $5\sigma_{\text{ff}}$, and R indicates the pairwise distances r_{ij} , z_{ik} , and h_{kl} . The total potential energy of the system, U , is described as

$$U = U^{\text{ff}} + U^{\text{fs}} + U^{\text{ss}}, \quad (5)$$

$$U^{\text{ff}} = \sum_{i=1}^{N-1} \sum_{j=i+1}^N u^{\text{ff}}(r_{ij}), \quad (6)$$

$$U^{\text{fs}} = \sum_{i=1}^N \sum_{k=-N_{\text{L}}/2}^{N_{\text{L}}/2-1} u^{\text{fs}}(z_{ik}), \quad (7)$$

$$U^{\text{ss}} = \sum_{k=-N_{\text{L}}/2}^{N_{\text{L}}/2-2} \sum_{l=k+1}^{N_{\text{L}}/2-1} u^{\text{ll}}(h_{kl}) + \sum_{k=-N_{\text{L}}/2}^{N_{\text{L}}/2-2} \sum_{m=k+1}^{N_{\text{L}}/2-1} u^{\text{pl}}(z_{km}) + \sum_{m=-N_{\text{L}}/2}^{N_{\text{L}}/2-2} \sum_{n=m+1}^{N_{\text{L}}/2-1} u^{\text{pp}}(r_{mn}), \quad (8)$$

where N and N_{L} are the numbers of the guest molecules and the layers, respectively. For a real PCP, electrostatic interactions should contribute to the configurational potential U^{ss} , but the interaction potential may be approximately reproduced, e.g., by tuning the LJ parameter ϵ_{ss} . Hence, electrostatic interactions are not considered in our model for the sake of simplicity. The stable interlayer width, h_0^* ($=h_0/\sigma_{\text{ff}}$), can be determined by Eq. (8) to be 1.75. The unit cell size was $10\sigma_{\text{ff}} \times 10\sigma_{\text{ff}}$ in the x - y layer directions and $1.60\sigma_{\text{ff}} - 2.05\sigma_{\text{ff}}$ in the z direction normal to the layers (thus, the z length of the simulation box is $11.20\sigma_{\text{ff}} - 14.35\sigma_{\text{ff}}$). Periodic boundary conditions were imposed for all directions.

The GCMC simulations were conducted for various interlayer widths ($1.60\sigma_{\text{ff}} - 2.05\sigma_{\text{ff}}$) with a step size Δh of $0.01\sigma_{\text{ff}}$. The length of the simulation run was 2.5×10^7 steps for equilibration and at least 2×10^8 steps for sampling.

B. Free-energy analysis

In this study, the relative osmotic free energy, $\Delta\Omega^{\text{OS}}$, was calculated by two alternative pathways. One was the thermodynamic integration of “imaginary” adsorption isotherms for the interlayer width h , which were obtained from the GCMC simulations.^{70,98} In this case, the osmotic free energy, Ω^{OS} , is represented by

$$\Omega^{\text{OS}}(\mu, h) = F^{\text{host}}(h) + PV(h) - \int_{-\infty}^{\mu} d\mu' N(\mu', h), \quad (9)$$

where F^{host} is the Helmholtz free energy of the host. P is the bulk pressure, $V(h)$ is the system volume at the interlayer width h , and $N(\mu, h)$ represents the imaginary adsorption isotherm. The relative osmotic free energy for the change

of the interlayer width from h_0 to h is given by

$$\Delta\Omega^{\text{OS}}(\mu, h) = \Omega^{\text{OS}}(\mu, h) - \Omega^{\text{OS}}(\mu, h_0), \quad (10)$$

where the relative Helmholtz energy of the host, $\Delta F^{\text{host}}(h) = F^{\text{host}}(h) - F^{\text{host}}(h_0)$ in Eq. (10), was approximated to the difference in the interlayer potential, $\Delta U^{\text{ss}}(h) = U^{\text{ss}}(h) - U^{\text{ss}}(h_0)$. This could be reasonable because the thermal fluctuation of the layer itself will change very little in this system upon the variation in the interlayer width, and thus, the term of the entropy change in $\Delta F^{\text{host}}(h)$ can be negligibly small. Then, the entropy change of the guest molecules against the interlayer width is included in the thermodynamic integration of the adsorption isotherm of Eq. (9), and it does not affect $\Delta F^{\text{host}}(h)$ itself.

Another route to obtain $\Delta\Omega^{\text{OS}}$ is the thermodynamic integration of the adsorption stress, σ_{ads} , with respect to the interlayer width

$$\Delta\Omega^{\text{OS}}(\mu, h) = -A \int_{h_0}^h dh' \sigma_{\text{ads}}(\mu, h'), \quad (11)$$

where A is the area of the layer. To calculate the adsorption stress, we derived the following three equivalent equations:

$$\sigma_{\text{ads}} = \frac{\langle F_z^{\text{fs}} \rangle + \langle F_z^{\text{ff}} \rangle + F_z^{\text{ss}}}{A} - P, \quad (12)$$

$$\sigma_{\text{ads}} = -\frac{\langle N \rangle k_B T}{V} + \frac{\langle W_{zz}^{\text{fs}} \rangle + \langle W_{zz}^{\text{ff}} \rangle}{V} + \frac{F_z^{\text{ss}}}{A} - P, \quad (13)$$

$$\begin{aligned} \sigma_{\text{ads}} = & \sum_{k=-N_L/2}^{N_L/2-1} \frac{k}{2} \int_0^h dz \int_{kh}^{(k+1)h} dz_k \\ & \times \left[-8\pi \varepsilon_{\text{ff}} \sigma_{\text{ff}} \langle \rho(z) \rangle \langle \rho(z_k) \rangle \left\{ \left(\frac{\sigma_{\text{ff}}}{z - z_k - kh} \right)^{11} \right. \right. \\ & \left. \left. - \left(\frac{\sigma_{\text{ff}}}{z - z_k - kh} \right)^5 \right\} \right] \\ & - \sum_{k=-N_L/2}^{N_L/2-1} k \int_0^h dz \left[-8\pi \rho_s \varepsilon_{\text{fs}} \sigma_{\text{fs}} \langle \rho(z) \rangle \left\{ \left(\frac{\sigma_{\text{fs}}}{z - kh} \right)^{11} \right. \right. \\ & \left. \left. - \left(\frac{\sigma_{\text{fs}}}{z - kh} \right)^5 \right\} \right] + \frac{F_z^{\text{ss}}}{A} - P, \quad (14) \end{aligned}$$

where the angle brackets denote an ensemble average. Equation (12) indicates that the adsorption stress can be calculated as the sum of the negative bulk pressure and the z components of the forces, F_z^{ff} , F_z^{fs} , and F_z^{ss} , derived from the fluid-fluid, fluid-solid, and solid-solid interaction potentials U^{ff} , U^{fs} , and U^{ss} , respectively. It is worth noting that the definition of adsorption stress in Eq. (12) is different from that of Neimark *et al.*,⁷³ in that the stress for the host deformation (F_z^{ss}/A) is included in our definition. The adsorption stress can be also obtained with Eq. (13) based on the virial theorem. The pressure of the confined fluid is calculated as the sum of the ideal gas pressure and the fluid-fluid and the fluid-solid virials applied in a direction normal to the layer, W_{zz}^{ff} and W_{zz}^{fs} , respectively. In Eq. (14), the local density profile of the guest

molecule, $\rho(z)$, is integrated to calculate the fluid-fluid and the fluid-solid interaction forces. In this equation, the guest molecules are assumed to have uniform density along the layer direction. By comparing the computational results, we confirmed that Eqs. (12)–(14) give the same adsorption stress. The details of the derivations of the three equations are described in the supplementary material.⁹⁷

III. RESULTS AND DISCUSSION

A. Equilibrium transition behavior

Figure 2 shows the relative osmotic free-energy profiles along the interlayer width for different relative pressures at a temperature of T^* ($=k_B T/\varepsilon_{\text{ff}}$) = 0.8, which were calculated by thermodynamic integration of the adsorption stress using Eqs. (11) and (12). At zero pressure, a global minimum is located at $h = h_0$ (closed state), which is determined by the balance between the interlayer attraction and the layer-pillar repulsion. The system becomes monotonically unstable with layer opening because the layers are forcibly drawn apart against the interlayer attractive force. At a pressure of $P/P_0 = 0.010$, a local minimum appears at h^* ($=h/\sigma_{\text{ff}}$) = 1.99, which is caused by stabilization due to the guest adsorption. A further increase in the pressure naturally increases the adsorbed amount of guest particles, making the state more stable. At $P/P_0 = 0.013$, the profile becomes bistable, which indicates that the closed state and the opened state ($h^* = 1.99$) are in thermodynamic equilibrium. The global minimum turns into the opened state from the closed state at pressures higher than the equilibrium transition pressure.

Figure 3 shows the relative osmotic free energies as a function of pressure for various fixed interlayer widths at $T^* = 0.8$ calculated by the other integration pathway (Eqs. (9) and (10)). The profile for $h^* = 1.75$ is independent of the pressure because no guests are adsorbed due to the narrow interlayer space and the contribution of $P\Delta V$ -term is negligible. At zero pressure, the closed state is the most stable and

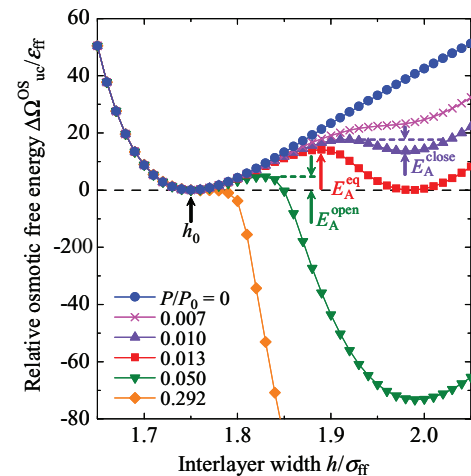


FIG. 2. Relative osmotic free energies as a function of interlayer width and pressure at T^* ($=k_B T/\varepsilon_{\text{ff}}$) = 0.8. E_A^{eq} , E_A^{open} , and E_A^{close} are the activation energies for the equilibrium transition and the spontaneous gate-opening and -closing transitions, respectively.

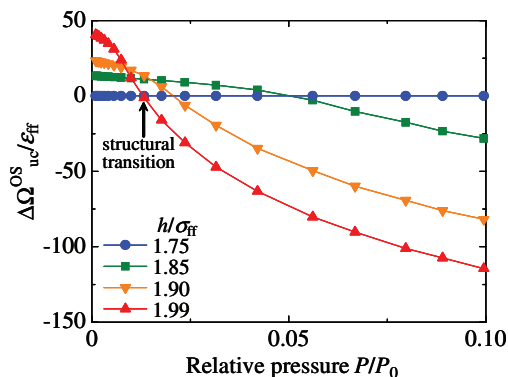


FIG. 3. Relative osmotic free energies as a function of pressure and interlayer width at $T^* = 0.8$.

the system with the larger interlayer width is unstable. Even at low pressures, the closed state is the most stable; however, the stable state shifts from the closed state ($h_0^* = 1.75$) to the opened state ($h^* = 1.99$) at $P/P_0 = 0.013$. The structural transition pressure determined by the thermodynamic integration of the adsorption isotherm is exactly the same with the transition pressure given by the above-mentioned thermodynamic integration (Eqs. (11) and (12)). The switch of the global minimum, which induces the structural transition and the guest adsorption, naturally yields a stepwise adsorption isotherm, as shown in Fig. 4. From these results, it is revealed that the equilibrium behavior of the adsorption-induced structural transition is dominated by the balance between two conflicting contributions: The energy penalty by the host expansion against the interlayer attraction and the stabilization due to the guest adsorption.

B. Hysteretic transition behavior

In Sec. III A, it is described how the equilibrium structural transition pressure was determined by equating the relative osmotic free energies of the closed and the opened states. However, the structural transition does not occur at the equilibrium transition pressure if the system cannot overcome the energy barrier located between the two stable states during a finite observation time. As shown in Fig. 2, the activa-

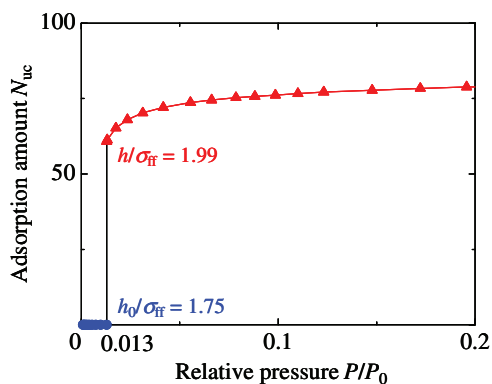


FIG. 4. Stepwise adsorption isotherm for the stack-layer PCP model due to the equilibrium structural transition from the interlayer width h/σ_{ff} of 1.75 (closed state) to 1.99 (opened state).

tion energy for the equilibrium transition, E_A^{eq} , is obtained from the free-energy difference between the two stable states ($h^* = 1.75$ and 1.99) and the transition state ($h^* = 1.89$ at $T^* = 0.8$). The activation energies of the gate-opening and -closing transitions, E_A^{open} and E_A^{close} , are also determined from the free-energy landscape: The free-energy difference between the closed state and the transition state (e.g., $h^* = 1.83$ at $P/P_0 = 0.050$) is the gate-opening activation energy. The activation energy for the gate opening disappears at $P/P_0 = 0.292$, which indicates the pressure of the metastable limit for the gate-opening transition. For the gate-closing process, the activation energy is obtained as the energy difference between the opened state and the transition state (for example, the difference between the opened state with $h^* = 1.99$ and the transition state with $h^* = 1.92$ at $P/P_0 = 0.010$), and the metastable limit of the gate closing is $P/P_0 = 0.007$. The pressure dependence of the activation energies, E_A^{open} and E_A^{close} , is shown in Fig. 5(a). The spontaneous transition pressures can be determined by assuming the system energy fluctuation and finding intersections of it with the E_A^{open} and E_A^{close} profiles. Here, if we assume the energy fluctuation is $6k_B T/uc$ (where uc denotes a unit cell), the hysteretic adsorption isotherm is determined as shown in Fig. 5(b). The gate-closing pressure is closer to the equilibrium transition pressure than the gate-opening pressure because the gate-closing activation energy is more sensitive to the bulk gas pressure. The difference in the pressure dependences between the gate-opening and -closing transitions reflects the difference in the respective mechanisms of spontaneous structural transition. In gate opening, the expansion of the interlayer width is the activation process, which requires a high pressure in order for guests to be adsorbed in the narrow pore space. However, in gate closing, the activation process is

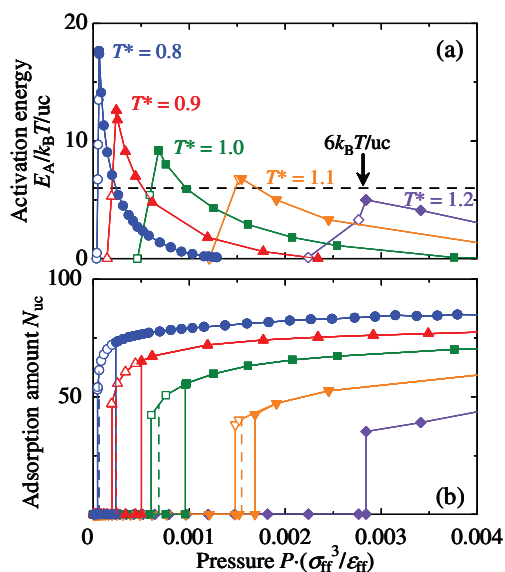


FIG. 5. (a) Pressure dependence of the activation energy of the structural transition for various temperatures of $T^* = 0.8$ –1.2. Closed and open symbols indicate the activation energies for the gate opening and the gate closing, respectively. The broken line represents the assumed system energy fluctuation of $6k_B T$ per unit cell. (b) Adsorption (closed symbol) and desorption (opened symbol) isotherms for various temperatures ($T^* = 0.8$ –1.2, the same colors as in (a)). The broken line indicates the equilibrium transition pressure.

the guest desorption from the widened pore space, which is sensitive to the bulk gas pressure. In this manner, free-energy analysis can be used to demonstrate the hysteretic adsorption behavior by considering the relation between the system energy fluctuation and the activation energy for the structural transition.

Figure 5(b) also shows temperature dependence of the adsorption isotherm. The hysteresis loop, which comes from the different gate-opening and -closing pressures, becomes wide with increasing temperature from $T^* = 0.8$ to 1.0, while it decreases in width at $T^* = 1.0$ and finally vanishes at $T^* = 1.2$. The dissipation of the hysteresis loop is due to the energy fluctuation of the system being larger than the activation energy even at the equilibrium transition pressure (see Fig. 5(a)). In experimental studies,^{7,12,17,20} only the increase in the hysteresis loop with increasing temperature was reported, and thus, this is the first time the non-monotonic temperature dependence of the hysteresis loop has been shown for the gate phenomenon. The non-monotonic temperature dependence found in this study may sound somehow surprising, because it is generally considered that the hysteresis loop due to the capillary condensation in mesopores is monotonically decreased with increasing temperature.^{99,100} However, the hysteresis loop due to the capillary condensation, which is caused by the different mechanism from the gate phenomenon, also shows the non-monotonic temperature dependence if the width of the hysteresis loop is expressed by the absolute pressure as in this study, not by the relative pressure.

As mentioned above, the hysteric behavior in the spontaneous adsorption-induced structural transition is dominated by the energy fluctuation of the system to overcome the energy barrier that separates the stable and metastable states. The energy fluctuation of the system should depend on the observation time and the size of a local domain in the PCP crystal. Thus, to estimate the energy fluctuation and determine the spontaneous gate-opening and -closing pressures, we constructed a kinetic transition model, as shown in Fig. 6. In this model, the PCP crystal is composed of small domains, and friction between them is neglected. According to the transition state theory, the rate constant of the gate-opening transition, k_{op} , can be obtained as

$$k_{op}(P, s_N) = \frac{1}{2} \sqrt{\frac{2k_B T}{\pi m}} \cdot \frac{\exp(-\beta \Delta \Omega_{uc}^{OS}(P, h) \cdot s_N) \Big|_{\text{transition state}}}{\int_{\text{closed}} dh \exp(-\beta \Delta \Omega_{uc}^{OS}(P, h) \cdot s_N)}, \quad (15)$$

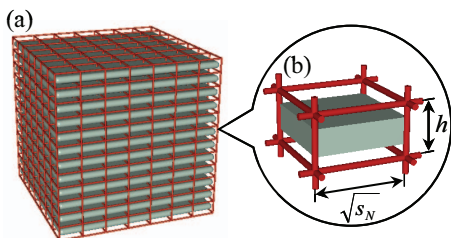


FIG. 6. Schematic representations of the kinetic transition model. (a) A PCP crystal, (b) a transition domain.

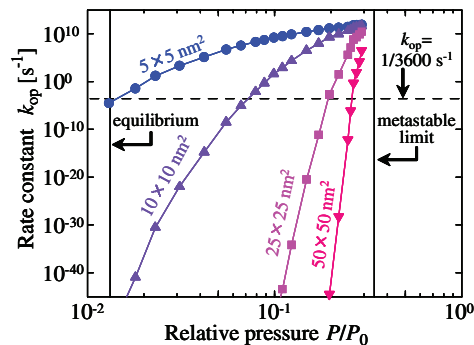


FIG. 7. Pressure dependence of the rate constant for the gate-opening transition at $T^* = 0.8$. Transition domain sizes are 5×5 , 10×10 , 25×25 , and 50×50 nm², respectively. The 2 vertical lines indicate the equilibrium transition pressure and the limit of the metastable pressure for the infinitely wide layer model. The horizontal broken line corresponds to $k_{op} = 1/3600$ s⁻¹.

where m and s_N denote the mass and area of the domain, respectively, and $\beta = 1/k_B T$. The rate constant k_{op} is the product of two contributions: the average velocity of the domain and the relative probability for the domain to be in the transition state. Figure 7 shows the pressure dependence of the rate constant for several sizes of the transition domain. The rate constant was calculated over the range from the equilibrium transition pressure to the metastable limit pressure for the infinitely wide layer model. The rate constant increases with increasing pressure by more than 15 orders of magnitude even for a domain size of 5×5 nm², and the increase becomes more drastic for larger domain sizes. A larger domain size tends to produce a smaller rate constant because a larger domain must overcome higher activation energy. Here, we set the observation time as one hour and assumed that spontaneous transition occurs at the pressure for which the time constant of the spontaneous transition $\tau_{op} (=1/k_{op})$ is equal to the observation time. Thus, the spontaneous transition pressure can be determined as the pressure at which the rate constant, k_{op} , reaches $1/3600$ s⁻¹ (broken line in Fig. 7). When the domain size is small, the structural transition tends to occur near the equilibrium transition pressure of the infinitely wide layer model. However, for a large domain, the structural transition occurs close to the metastable limit pressure of the infinitely wide layer model. The correlation between the domain size and the system energy fluctuation at $T^* = 0.8$ was obtained by the following scheme: First, the structural transition pressure at which the rate constant reaches $1/3600$ s⁻¹ was calculated as a function of the domain size. Second, the activation energies of the gate opening corresponding to the obtained structural transition pressures at $T^* = 0.8$ were determined from Fig. 5(b). The obtained activation energy could be regarded as the system energy fluctuation. Figure 8 shows the system energy fluctuation as a function of the domain size. The system energy fluctuation per the transition domain is about $35 k_B T$ and is nearly independent of the transition domain size; however, the system energy fluctuation per unit cell (see Fig. 1(c)) decreases with increasing domain size. The system energy fluctuation per unit cell shown in Fig. 8 indicates that the energy fluctuation of $6k_B T/uc$ assumed above corresponds to the transition domain size of 8.3×8.3 nm². The volume

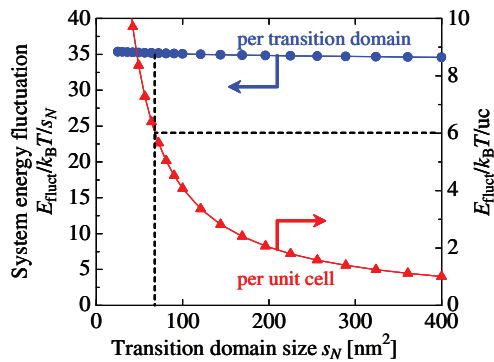


FIG. 8. System energy fluctuation per one transition domain (blue circle, left vertical axis), and per unit cell (red triangle, right axis) as a function of transition domain size for an observation time of one hour at $T^* = 0.8$. The vertical broken line indicates the domain size corresponding to the assumed system energy fluctuation of $6 k_B T/luc$ in Sec. III B.

of the transition domain can be calculated as $8.3 \times 8.3 \times l_z = 43 \text{ nm}^3$ (where l_z is the interlayer width of 0.62 nm in the activation state), and the corresponding energy fluctuation per unit cell is $35 k_B T$. These values seem reasonable considering the activation energy of $59 k_B T$ for the nucleation of a liquid droplet of 336 LJ particles (17 nm^3 in volume) from a vapor phase.¹⁰¹

C. Temperature dependence of the structural transition pressures

Many experimental studies obtained a linear correlation between the logarithm of the gate-opening pressure (and/or -closing transition pressure) vs. reciprocal temperature^{6,8,11,12,96} and the slope of the plot of $\ln P$ vs. T^{-1} could be considered as structural transition enthalpies based on the Clausius-Clapeyron equation.^{6,12} As shown in Fig. 9, our simulations also provide a linear correlation for the equilibrium structural transition and also for the spontaneous gate-opening and -closing transitions; however, the Clausius-Clapeyron equation should not be applied to spontaneous transitions, because it assumes phase equilibrium. Therefore, we constructed models to demonstrate the enthalpies obtained

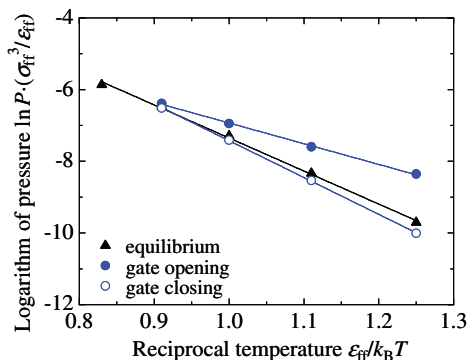


FIG. 9. Temperature dependence of the pressures for the equilibrium transition, the spontaneous gate-opening and -closing transitions. Lines were calculated by the least squares fitting. Obtained slopes are $-9.3\epsilon_{ff}$ (equilibrium), $-5.8\epsilon_{ff}$ (gate opening), and $-10.2\epsilon_{ff}$ (gate closing), respectively.

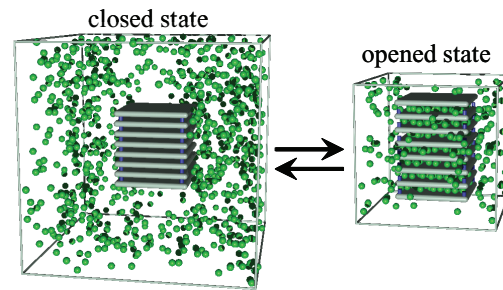


FIG. 10. Schematic illustration of the isothermal-isobaric system including a bulk gas phase and a PCP crystal. The closed state and the opened state are in equilibrium.

from the slopes of the plots of $\ln P$ vs. T^{-1} for the equilibrium transition and the spontaneous transitions.

In modeling the $\ln P$ vs. T^{-1} correlation for the equilibrium transition, we considered an isothermal-isobaric system that includes a PCP crystal and a bulk gas phase as shown in Fig. 10. Surface adsorption on the PCP crystal was neglected. When the system is in equilibrium between the closed and the opened states, the Gibbs free energies of the two states are balanced

$$G^{\text{closed}} = G^{\text{opened}}. \quad (16)$$

By taking the total derivative of both sides, we can obtain

$$\frac{dP}{dT} = \frac{\Delta H^{\text{trs}}}{T \Delta V^{\text{trs}}} = \frac{\Delta H^{\text{trs}}}{T(\Delta V_{\text{gas}} + \Delta V_{\text{PCP}})}, \quad (17)$$

where ΔH^{trs} is the enthalpy change during the structural transition and ΔV^{trs} is total volume change of the system, which is the sum of changes in volume of the gas phase and that of the PCP crystal due to the deformation induced by the gas adsorption, i.e., the sum of ΔV_{gas} and ΔV_{PCP} , respectively. Here, the ΔV_{PCP} term is negligible compared with ΔV_{gas} . By assuming the ideal gas law for the gas phase, the following equation can be obtained:

$$\frac{d \ln P}{d(T^{-1})} \cong \frac{\Delta H^{\text{trs}}}{k_B \Delta N}, \quad (18)$$

where ΔN is the change in the adsorbed amount of guest particles. Equation (18) shows that the slope of the plot of $\ln P$ vs. T^{-1} for the equilibrium structural transition provides the transition enthalpy per adsorbed guest molecule. This model was tested by comparing the slope of the plot with the transition enthalpies directly obtained from the GCMC simulations, as shown in Fig. 11. The directly obtained transition enthalpies were calculated as the difference between the post-transition state with an interlayer width of h and the pre-transition state (with an interlayer width of h_0 in this case)

$$\Delta H(h) = (\langle U^{\text{ff}} \rangle + \langle U^{\text{fs}} \rangle + U^{\text{ss}} + PV)|_h - (\langle U^{\text{ff}} \rangle + \langle U^{\text{fs}} \rangle + U^{\text{ss}} + PV)|_{\text{pre-trs}}. \quad (19)$$

As can be seen from Fig. 11, the slope of the plot of $\ln P$ vs. T^{-1} is in fairly good agreement with the directly obtained transition enthalpies. This demonstrates that the Clausius-Clapeyron type of analysis can be valid even for an adsorption-induced structural transition.

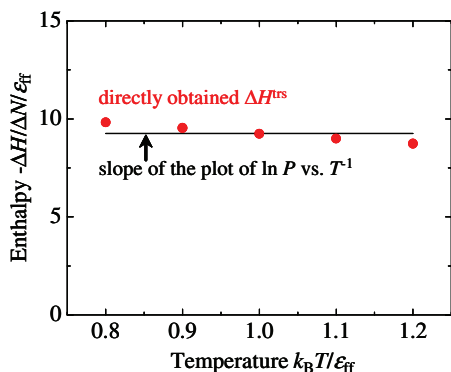


FIG. 11. Comparison of the slope of the plot of $\ln P$ vs. T^{-1} for the equilibrium transition and the transition enthalpies directly obtained from the GCMC simulations.

Furthermore, we also constructed a model for the $\ln P$ vs. T^{-1} correlation in the spontaneous (gate-opening and -closing) transitions from the metastable states. In this case, the correlation between the Gibbs free energies of the pre-transition state and the activation state, $G^{\text{pre-trs}}$ and G^{act} , respectively, can be written as

$$G^{\text{pre-trs}} + \Delta G = G^{\text{act}}, \quad (20)$$

where ΔG is the activation energy. Here, we define the following relation:

$$\frac{\Delta G}{k_B T} = \alpha, \quad (21)$$

where α is a constant. The total derivative of Eq. (20) is obtained as

$$\Delta V^{\text{act}} dP = (\Delta S^{\text{act}} + \alpha k_B) dT, \quad (22)$$

where ΔV^{act} and ΔS^{act} are changes in the volume and the entropy between the pre-transition and the activation states, respectively. By combining Eqs. (21) and (22) and applying the ideal gas law to the gas phase, the following equation for the spontaneous transitions is obtained:

$$\frac{d \ln P}{d(T^{-1})} \cong \frac{\Delta H^{\text{act}}}{k_B \Delta N^{\text{act}}}, \quad (23)$$

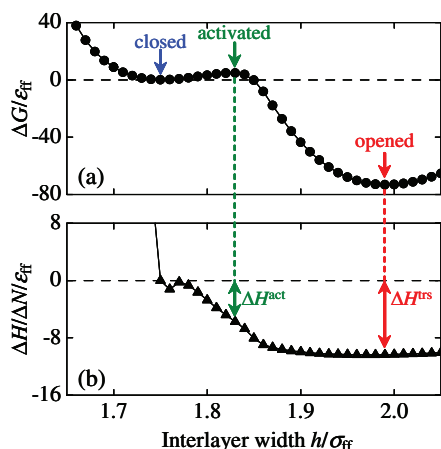


FIG. 12. (a) Relative Gibbs free energy and (b) relative enthalpy, as a function of interlayer width ($T^* = 0.8$, $P/P_0 = 0.050$).

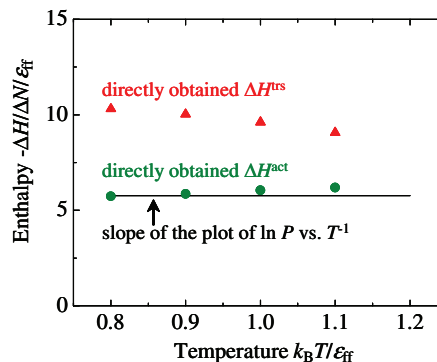


FIG. 13. Comparison of the slope of the plot of $\ln P$ vs. T^{-1} for the gate-opening transition, the transition enthalpies, ΔH^{trs} , and the activation enthalpies, ΔH^{act} , directly obtained from the GCMC simulations.

where ΔH^{act} and ΔN^{act} are the changes in the enthalpy and the adsorption amount between the pre-transition and the activation states, respectively. This model indicates that the slopes of the plot of $\ln P$ vs. T^{-1} for the spontaneous transitions give the activation enthalpies per adsorbed guest molecule at the activation state. To verify the model, we compared the slope of the gate-opening transition with the activation enthalpy ΔH^{act} and the transition enthalpy ΔH^{trs} obtained directly from the GCMC simulations. The ΔH^{act} and ΔH^{trs} values were obtained by the following scheme: First, the interlayer widths of the pre- and post-transition states and the activation state at $P/P_0 = 0.050$ and $T^* = 0.8$ were determined from the relative Gibbs free-energy profile shown in Fig. 12(a). Second, ΔH^{act} and ΔH^{trs} at the interlayer widths of the activation and the post-transition states were extracted from the enthalpy change profile obtained by Eq. (19) (Fig. 12(b)). It is worth noting that the change in the Gibbs free energy of the system, including the PCP crystal and the bulk phase (Fig. 10), is the same as that in the free energy of the osmotic system (Fig. 1(d)). Figure 13 shows a comparison of the directly obtained activation and transition enthalpies and the slope of the plot of $\ln P$ vs. T^{-1} for the gate-opening transition. The slope is in good agreement with the directly obtained activation enthalpies, but clearly distinct from the transition enthalpies. We also conducted a similar verification of the model for gate-closing behavior by comparing the slope of the plot of $\ln P$ vs. T^{-1} with the directly obtained activation enthalpy, and a good agreement was obtained as is the case in the gate-opening behavior. This suggests that the slopes of the plots of $\ln P$ vs. T^{-1} for the spontaneous gate-opening and -closing transitions correspond to the activation enthalpies to reach the transient states, not the transition enthalpies getting to the final (opened and closed) states as reported in several experimental studies.

IV. CONCLUSION

In this study, we investigated the adsorption-induced structural transition of stacked-layer PCP based on free-energy analysis by thermodynamic integration of the GCMC simulation results. Our calculation showed that the global minimum changed from the closed state into the opened state

with increasing pressure, which indicates that the equilibrium adsorption-induced structural transition is dominated by the balance between the energy cost of the host deformation and the stabilization due to the guest adsorption. The free-energy analysis also provided the spontaneous structural transition pressures by calculating the activation energy from the free-energy profile and by assuming the system energy fluctuation. The hysteresis loop shows the non-monotonic temperature dependence: at low temperature, the hysteresis loop increases with rising temperature as observed in many experiments, but it eventually decreases at even higher temperatures and finally vanishes. To estimate the system energy fluctuation, the kinetic transition model was proposed, and the rate constant for the gate opening at an observation time of one hour was evaluated as a function of the size of the transition domain. A smaller domain size produces a transition pressure closer to the equilibrium transition pressure, whereas for a larger domain size, the transition tends to occur near the pressure of the metastable limit. We also constructed the two models to demonstrate the enthalpies obtained from the slopes of the plot of $\ln P$ vs. T^{-1} for the equilibrium transition and the spontaneous transitions, and we tested the models by comparing them with the enthalpies directly obtained from the GCMC simulations. The model for equilibrium transition demonstrated that the slope of the plot of $\ln P$ vs. T^{-1} for the equilibrium transition provided the transition enthalpy per adsorbed guest molecule. However, the model for spontaneous transitions indicated that the slopes represented the activation enthalpy per adsorbed guest molecule in the activation state. These models give us a clear understanding of the temperature-pressure correlation in adsorption-induced structural transitions.

ACKNOWLEDGMENTS

R.N. acknowledges Professor A. V. Neimark for fruitful discussion. This work was supported by a Grant-in-Aid for Scientific Research (B) No. 21360379 from MEXT. R.N. thanks the JSPS Research Fellowship and the Global Center of Excellence (GCOE) Program.

- ¹S. Kitagawa, R. Kitaura, and S. Noro, *Angew. Chem., Int. Ed.* **43**, 2334 (2004).
- ²J. L. C. Rowsell and O. M. Yaghi, *Microporous Mesoporous Mater.* **73**, 3 (2004).
- ³M. J. Rosseinsky, *Microporous Mesoporous Mater.* **73**, 15 (2004).
- ⁴S. Horike, S. Shimomura, and S. Kitagawa, *Nat. Chem.* **1**, 695 (2009).
- ⁵C. Serre, F. Millange, C. Thouvenot, M. Nogues, G. Marsolier, D. Louer, and G. Ferey, *J. Am. Chem. Soc.* **124**, 13519 (2002).
- ⁶S. Takamizawa, E. Nakata, and H. Yokoyama, *Inorg. Chem. Commun.* **6**, 763 (2003).
- ⁷S. Takamizawa, Y. Takasaki, and R. Miyake, *Chem. Commun.* **2009**, 6625.
- ⁸S. Takamizawa, E. Nakata, T. Akatsuka, R. Miyake, Y. Kakizaki, H. Takeuchi, G. Maruta, and S. Takeda, *J. Am. Chem. Soc.* **132**, 3783 (2010).
- ⁹R. Kitaura, K. Seki, G. Akiyama, and S. Kitagawa, *Angew. Chem., Int. Ed.* **42**, 428 (2003).
- ¹⁰K. Uemura, S. Kitagawa, K. Fukui, and K. Saito, *J. Am. Chem. Soc.* **126**, 3817 (2004).
- ¹¹K. Uemura, S. Kitagawa, K. Saito, K. Fukui, and K. Matsumoto, *J. Therm. Anal. Calorim.* **81**, 529 (2005).
- ¹²H. Noguchi, A. Kondo, Y. Hattori, H. Kanoh, H. Kajiro, and K. Kaneko, *J. Phys. Chem. B* **109**, 13851 (2005).
- ¹³A. Kondo, H. Noguchi, S. Ohnishi, H. Kajiro, A. Tohdoh, Y. Hattori, W.-C. Xu, H. Tanaka, H. Kanoh, and K. Kaneko, *Nano Lett.* **6**, 2581 (2006).
- ¹⁴A. Kondo, H. Noguchi, L. Carlucci, D. M. Proserpio, G. Ciani, H. Kajiro, T. Ohba, H. Kanoh, and K. Kaneko, *J. Am. Chem. Soc.* **129**, 12362 (2007).
- ¹⁵S. Horike, D. Tanaka, K. Nakagawa, and S. Kitagawa, *Chem. Commun.* **2007**, 3395.
- ¹⁶A. Kondo, A. Chinen, H. Kajiro, T. Nakagawa, K. Kato, M. Takata, Y. Hattori, F. Okino, T. Ohba, K. Kaneko, and H. Kanoh, *Chem.-Eur. J.* **15**, 7549 (2009).
- ¹⁷H. Kanoh, A. Kondo, H. Noguchi, H. Kajiro, A. Tohdoh, Y. Hattori, W.-C. Xu, M. Inoue, T. Sugiura, K. Morita, H. Tanaka, T. Ohba, and K. Kaneko, *J. Colloid Interface Sci.* **334**, 1 (2009).
- ¹⁸K. Nakagawa, D. Tanaka, S. Horike, S. Shimomura, M. Higuchi, and S. Kitagawa, *Chem. Commun.* **46**, 4258 (2010).
- ¹⁹H. Kajiro, A. Kondo, K. Kaneko, and H. Kanoh, *Int. J. Mol. Sci.* **11**, 3803 (2010).
- ²⁰K. Seki, *Phys. Chem. Chem. Phys.* **4**, 1968 (2002).
- ²¹K. Uemura, Y. Yamasaki, Y. Komagawa, K. Tanaka, and H. Kita, *Angew. Chem., Int. Ed.* **46**, 6662 (2007).
- ²²K. Uemura, F. Onishi, Y. Yamasaki, and H. Kita, *J. Solid State Chem.* **182**, 2852 (2009).
- ²³T. Duren, L. Sarkisov, O. M. Yaghi, and R. Q. Snurr, *Langmuir* **20**, 2683 (2004).
- ²⁴T. Duren and R. Q. Snurr, *J. Phys. Chem. B* **108**, 15703 (2004).
- ²⁵N. Yanai, K. Kitayama, Y. Hijikata, H. Sato, R. Matsuda, Y. Kubota, M. Takata, M. Mizuno, T. Uemura, and S. Kitagawa, *Nat. Mater.* **10**, 787 (2011).
- ²⁶T. Uemura, D. Hiramatsu, Y. Kubota, M. Takata, and S. Kitagawa, *Angew. Chem., Int. Ed.* **46**, 4987 (2007).
- ²⁷P. Horcajada, C. Serre, M. Vallet-Regi, M. Sebban, F. Taulelle, and G. Ferey, *Angew. Chem., Int. Ed.* **45**, 5974 (2006).
- ²⁸C. Serre, S. Bourrelly, A. Vimont, N. A. Ramsahye, G. Maurin, P. L. Llewellyn, M. Daturi, Y. Filinchuk, O. Leynaud, P. Barnes, and G. Ferey, *Adv. Mater.* **19**, 2246 (2007).
- ²⁹R. W. Mooney, A. G. Keenan, and L. A. Wood, *J. Am. Chem. Soc.* **74**, 1371 (1952).
- ³⁰R. W. Mooney, A. G. Keenan, and L. A. Wood, *J. Am. Chem. Soc.* **74**, 1367 (1952).
- ³¹J.-M. Cases, I. Berend, G. Besson, M. Francois, J.-P. Uriot, F. Thomas, and J. E. Poirier, *Langmuir* **8**, 2730 (1992).
- ³²I. Berend, J.-M. Cases, M. Francois, J.-P. Uriot, L. Michot, A. Masion, and F. Thomas, *Clays Clay Miner.* **43**, 324 (1995).
- ³³J.-M. Cases, I. Berend, M. Francois, J.-P. Uriot, L. J. Michot, and F. Thomas, *Clays Clay Miner.* **45**, 8 (1997).
- ³⁴C. A. Fyfe, Y. Feng, H. Grondey, and G. T. Kokotailo, *J. Chem. Soc., Chem. Commun.* **1990**, 1224.
- ³⁵D. H. Olson, G. T. Kokotailo, S. L. Lawton, and W. M. Meier, *J. Phys. Chem.* **85**, 2238 (1981).
- ³⁶J. Trudel, S. Hosatte, and M. Ternan, *Appl. Therm. Eng.* **19**, 495 (1999).
- ³⁷C. Y. Liu and K. Aika, *Ind. Eng. Chem. Res.* **43**, 6994 (2004).
- ³⁸C. Y. Liu and K. Aika, *Bull. Chem. Soc. Jpn.* **77**, 123 (2004).
- ³⁹T. Dewa, K. Endo, and Y. Aoyama, *J. Am. Chem. Soc.* **120**, 8933 (1998).
- ⁴⁰W. J. V. Meegen and I. K. Snook, *J. Chem. Phys.* **74**, 1409 (1981).
- ⁴¹I. K. Snook and W. V. Meegen, *J. Chem. Phys.* **72**, 2907 (1980).
- ⁴²J. E. Lane and T. H. Spurling, *Chem. Phys. Lett.* **67**, 107 (1979).
- ⁴³R. M. Pashley and J. N. Israelachvili, *J. Colloid Interface Sci.* **101**, 511 (1984).
- ⁴⁴R. G. Horn and J. N. Israelachvili, *Chem. Phys. Lett.* **71**, 192 (1980).
- ⁴⁵R. Evans and U. M. B. Marconi, *J. Chem. Phys.* **86**, 7138 (1987).
- ⁴⁶M. Schoen, D. J. Diestler, and J. H. Cushman, *J. Chem. Phys.* **87**, 5464 (1987).
- ⁴⁷P. B. Balbuena, D. Berry, and K. E. Gubbins, *J. Phys. Chem.* **97**, 937 (1993).
- ⁴⁸D. J. Diestler, M. Schoen, and J. H. Cushman, *Science* **262**, 545 (1993).
- ⁴⁹D. J. Diestler, M. Schoen, J. E. Curry, and J. H. Cushman, *J. Chem. Phys.* **100**, 9140 (1994).
- ⁵⁰M. Schoen, D. J. Diestler, and J. H. Cushman, *J. Chem. Phys.* **100**, 7707 (1994).
- ⁵¹M. Schoen, S. Hess, and D. J. Diestler, *Phys. Rev. E* **52**, 2587 (1995).
- ⁵²D. J. Diestler and M. Schoen, *J. Chem. Phys.* **104**, 6784 (1996).
- ⁵³T. Gruhn and M. Schoen, *Phys. Rev. E* **55**, 2861 (1997).

- ⁵⁴P. Bordarier, B. Rousseau, and A. H. Fuchs, *J. Chem. Phys.* **106**, 7295 (1997).
- ⁵⁵F. Porcheron, B. Rousseau, A. H. Fuchs, and M. Schoen, *Phys. Chem. Chem. Phys.* **1**, 4083 (1999).
- ⁵⁶F. Porcheron, M. Schoen, and A. H. Fuchs, *J. Chem. Phys.* **116**, 5816 (2002).
- ⁵⁷N. T. Skipper, K. Refson, and J. D. C. McConnell, *J. Chem. Phys.* **94**, 7434 (1991).
- ⁵⁸A. Delville and S. Sokolowski, *J. Phys. Chem.* **97**, 6261 (1993).
- ⁵⁹E. S. Boek, P. V. Coveney, and N. T. Skipper, *J. Am. Chem. Soc.* **117**, 12608 (1995).
- ⁶⁰E. S. Boek, P. V. Coveney, and N. T. Skipper, *Langmuir* **11**, 4629 (1995).
- ⁶¹N. T. Skipper, F.-R. C. Chang, and G. Sposito, *Clays Clay Miner.* **43**, 285 (1995).
- ⁶²N. T. Skipper, G. Sposito, and F.-R. C. Chang, *Clays Clay Miner.* **43**, 294 (1995).
- ⁶³A. V. C. De Siqueira, N. T. Skipper, P. V. Coveney, and E. S. Boek, *Mol. Phys.* **92**, 1 (1997).
- ⁶⁴M. Chavez-Paez, K. V. Workum, L. D. Pablo, and J. J. D. Pablo, *J. Chem. Phys.* **114**, 1405 (2001).
- ⁶⁵M. Chavez-Paez, L. D. Pablo, and J. J. D. Pablo, *J. Chem. Phys.* **114**, 10948 (2001).
- ⁶⁶A. Delville, *J. Phys. Chem.* **97**, 9703 (1993).
- ⁶⁷S. Karaborni, B. Smit, W. Heidug, J. Urai, and E. Van Oort, *Science* **271**, 1102 (1996).
- ⁶⁸A. Ghoufi, G. Maurin, and G. Ferey, *J. Phys. Chem. Lett.* **1**, 2810 (2010).
- ⁶⁹A. Ghoufi and G. Maurin, *J. Phys. Chem. C* **114**, 6496 (2010).
- ⁷⁰F.-X. Coudert, M. Jeffroy, A. H. Fuchs, A. Boutin, and C. Mellot-Draznieks, *J. Am. Chem. Soc.* **130**, 14294 (2008).
- ⁷¹F.-X. Coudert, C. Mellot-Draznieks, A. H. Fuchs, and A. Boutin, *J. Am. Chem. Soc.* **131**, 11329 (2009).
- ⁷²A. Boutin, M.-A. Springuel-Huet, A. Nossouf, A. Gedeon, T. Loiseau, C. Volkringer, G. Ferey, F.-X. Coudert, and A. H. Fuchs, *Angew. Chem., Int. Ed.* **48**, 8314 (2009).
- ⁷³A. V. Neimark, F.-X. Coudert, A. Boutin, and A. H. Fuchs, *J. Phys. Chem. Lett.* **1**, 445 (2010).
- ⁷⁴A. V. Neimark, F.-X. Coudert, C. Triguero, A. Boutin, A. H. Fuchs, I. Beurroies, and R. Denoyel, *Langmuir* **27**, 4734 (2011).
- ⁷⁵A. Boutin, F.-X. Coudert, M.-A. Springuel-Huet, A. V. Neimark, G. R. Feérey, and A. H. Fuchs, *J. Phys. Chem. C* **114**, 22237 (2010).
- ⁷⁶C. Triguero, F.-X. Coudert, A. Boutin, A. H. Fuchs, and A. V. Neimark, *J. Phys. Chem. Lett.* **2**, 2033 (2011).
- ⁷⁷F.-X. Coudert, A. Boutin, M. Jeffroy, C. Mellot-Draznieks, and A. H. Fuchs, *ChemPhysChem* **12**, 247 (2011).
- ⁷⁸S. Watanabe, H. Sugiyama, H. Adachi, H. Tanaka, and M. T. Miyahara, *J. Chem. Phys.* **130**, 164707 (2009).
- ⁷⁹H. Sugiyama, S. Watanabe, H. Tanaka, and M. T. Miyahara, *Langmuir* **28**, 5093 (2012).
- ⁸⁰D. E. Smith, *Langmuir* **14**, 5959 (1998).
- ⁸¹R. M. Shroll and D. E. Smith, *J. Chem. Phys.* **111**, 9025 (1999).
- ⁸²D. A. Young and D. E. Smith, *J. Phys. Chem. B* **104**, 9163 (2000).
- ⁸³E. J. M. Hensen, T. J. Tambach, A. Bliiek, and B. Smit, *J. Chem. Phys.* **115**, 3322 (2001).
- ⁸⁴E. J. M. Hensen and B. Smit, *J. Phys. Chem. B* **106**, 12664 (2002).
- ⁸⁵T. J. Tambach, E. J. M. Hensen, and B. Smit, *J. Phys. Chem. B* **108**, 7586 (2004).
- ⁸⁶H. D. Whitley and D. E. Smith, *J. Chem. Phys.* **120**, 5387 (2004).
- ⁸⁷T. J. Tambach, P. G. Bolhuis, E. J. M. Hensen, and B. Smit, *Langmuir* **22**, 1223 (2006).
- ⁸⁸D. E. Smith, Y. Wang, A. Chaturvedi, and H. D. Whitley, *J. Phys. Chem. B* **110**, 20046 (2006).
- ⁸⁹D. Bousquet, F. X. Coudert, and A. Boutin, *J. Chem. Phys.* **137**, 044118 (2012).
- ⁹⁰R. Q. Snurr, A. T. Bell, and D. N. Theodorou, *J. Phys. Chem.* **98**, 5111 (1994).
- ⁹¹M. Jeffroy, A. H. Fuchs, and A. Boutin, *Chem. Commun.* **2008**, 3275.
- ⁹²M. Jeffroy, G. Weber, S. Hostachy, J.-P. Bellat, A. H. Fuchs, and A. Boutin, *J. Phys. Chem. C* **115**, 3854 (2011).
- ⁹³H. Eyring, *J. Chem. Phys.* **3**, 107 (1935).
- ⁹⁴D. Chandler, *J. Chem. Phys.* **68**, 2959 (1978).
- ⁹⁵P. R. ten Wolde, M. J. Ruiz-Montero, and D. Frenkel, *J. Chem. Phys.* **104**, 9932 (1996).
- ⁹⁶S. Takamizawa, T. Saito, T. Akatsuka, and E. Nakata, *Inorg. Chem.* **44**, 1421 (2005).
- ⁹⁷See supplementary material at <http://dx.doi.org/10.1063/1.4789810> for details of the derivations of Eqs. (3), (12)–(14).
- ⁹⁸B. K. Peterson and K. E. Gubbins, *Mol. Phys.* **62**, 215 (1987).
- ⁹⁹K. Morishige and Y. Nakamura, *Langmuir* **20**, 4503 (2004).
- ¹⁰⁰K. Morishige and M. Ito, *J. Chem. Phys.* **117**, 8036 (2002).
- ¹⁰¹P. R. ten Wolde, M. J. Ruiz-Montero, and D. Frenkel, *J. Chem. Phys.* **110**, 1591 (1999).